Electronic Supplementary Material (ESI) for RSC Advances.

Supporting information for "Spray Reaction Prepared $FA_{1-x}Cs_xPbI_3$ Solid Solution as Light Harvester for Perovskite Solar Cells with Improved Humidity Stability"

Xiang Xia,[a] Wenyi Wu,[b] Hongcui Li,[a] Bo Zheng,[a] Yebin Xue,[a] Jing Xu,[a] Dawei Zhang,[a] Chunxiao Gao[b] and Xizhe Liu*[a]

[a]*Laboratoryfor Applied Atomic and Molecular Spectroscopy, Institute of Atomic and Molecular Physics, Jilin University, Changchun 130012, P. R. China.*
[b]*State Key Laboratory for Superhard Materials, Jilin University, Changchun 130012, P. R. China.*

**Corresponding author.*
E-mail: liu_xizhe@jlu.edu.cn(Xizhe Liu)

1. Experimental Section

Device fabrication: Firstly, FTO glass (TEC-8, Pilkington) was etched by Zn/HCl and ultrasonic cleaned by acetone and ethanol. Then, compact TiO_2 film (c-TiO_2, ~30 nm in thickness) was deposited by spray pyrolysis with 1.0 mL 50 mmol/L $Ti(OPr)_2(AcAc)_2$ in ethanol solution at 450 ^oC. Mesoporous TiO_2 film (mp-TiO_2) was deposited on the c-TiO_2 film by spin-coating with ethanol diluted TiO_2 paste (18NRT, Dyesol) solution at 5000 rpm for 30 sec. The mass ratio of the original TiO_2 paste to ethanol is 1:6. Then, the sample was dried and sintered at 80 ^oC for 30 min, 125 ^oC for 30 min, 325 ^oC for 30 min, and 500 ^oC for 30 min. After further treatment with 40 mM $TiCl_4$ (Sinopharm, 98%) at 70 ^oC for 30 min, the sample was rinsed with water and ethanol, and sintered at 450 ^oC for 30 min. Certain amounts of CsI (Aldrich, 99.9%) were added in 462 mg/mL PbI_2 (Aldrich, 99%) N,N-Dimethylformamide (DMF) solution following the Cs/Pb ratio of $FA_{1-x}Cs_xPbI_3$ (x=0, 0.1, 0.2 and 0.3). This CsI/PbI_2 mixed solution or pure PbI_2 solution were spin-coated on the mesoporous TiO_2 film at 4000 rpm for 30 sec. After preheating at the reaction temperature for 5 min on a hot plate, 100 μL 50 mg/mL FAI (synthesized, literature 29) in isopropanol solution was sprayed on the top of the PbI_2 film by a nitrogen gas atomizing spray nozzle at 160 ^oC for the interface reaction. The spraying speed of FAI solution was constant (10 μL/s) and the flow rate of N_2 gas was also constant (200 L/h). The working distance between spray nozzle and PbI_2 film was 8 cm. After the interface reaction process, the film was washed with isopropanol and annealed at the same temperature with interface reaction for 10 min. $FA_{1-x}Cs_xPbI_3$ films were also prepared at different reaction temperatures between 120 ^oC and 200 ^oC. The hole conductor layer was then deposited by spin-coating at 4,000 rpm for 20 sec. The spin-coating solution was prepared by dissolving 72.3 mg (2,2',7,7'-tetrakis(N,N-di-p-methoxyphenylamine)-9,9-spirobifluorene) (spiro-MeOTAD) (Feiming Inc.), 28.8 μL 4-tert-butylpyridine (Aldrich, 96%) and 17.5 μL lithium bis(trifluoromethylsulphonyl)imide (Aldrich, 99.95%) solution (520 mg/mL in acetonitrile) in 1 mL chlorobenzene. After the hole conductor layer being aged in the dried air condition of a brown desiccator for 12 hours, gold top electrode was deposited to complete the device. All these operations were performed in air condition.

Measurement: The XRD spectra were obtained using a Rigaku D/max-2500 X-ray diffractometer. Absorption spectra were measured by an UV-VIS spectrometer (L6S, INESA). Photocurrent density-photovoltage characteristics were recorded from 1.1 V to 0 V by a CHI660 electrochemical workstation. The active area of solar cells was 0.15 cm^2, which defined by a mask. AM1.5 illumination was provided by a 3A class solar simulator (UHE-16,

ScienceTech Inc.), which was calibrated to one sun by a KG5 filtered Si reference solar cell (certificated by VLSI Standards Inc., traceable to National Renewable Energy Laboratory). IPCE spectra were measured in the DC mode by a controlled monochrometer (BOCIC Inc.) with a 500W Xe light source (NBet Inc.). The certificated Si cell (VLSI Standards Inc.) is used as the reference. Impedance spectra were measured under constant illumination condition over a frequency range of 100 kHz to 0.1 Hz by CHI660 electrochemical workstation. The applied bias voltage was from 900 mV to 0 mV and the constant illumination was obtained using a white LED lamp. The EDS and SEM experiments were performed by FEI MAGELLAN 400 Scanning Electron Microscope. The XPS spectra were performed by VG scientat XPS system. In the humidity stability test, the perovskite solar cells are not encapsulated and kept in dark condition. The devices are aged in the environment of 50% humidity at 20 °C for 100 h.

2. Figures

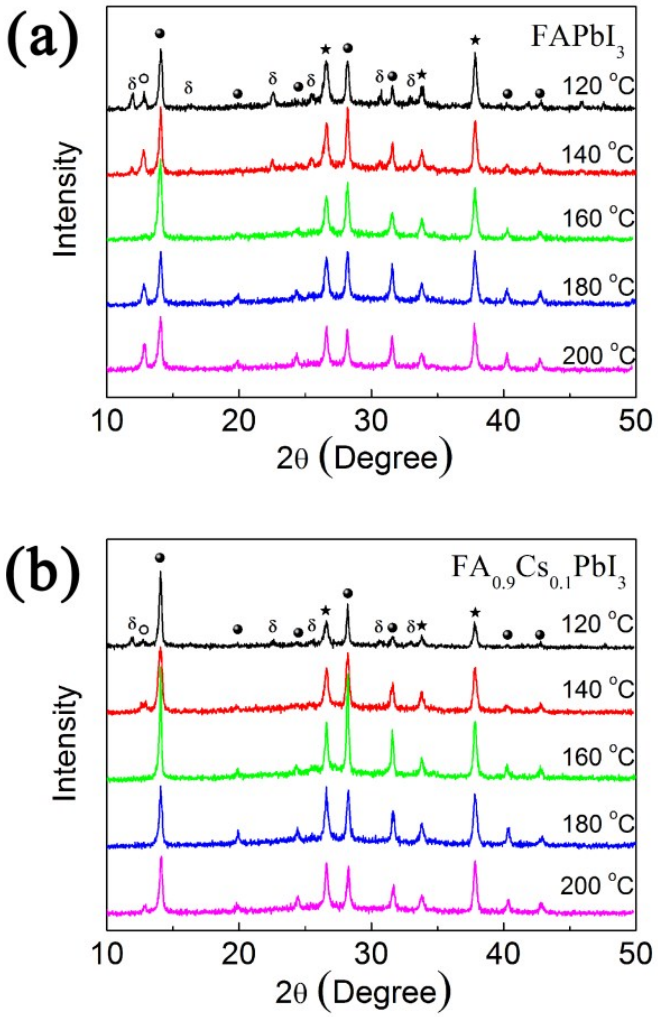

Fig. S1 The XRD patterns of the (a) $FAPbI_3$ and (b) $FA_{0.9}Cs_{0.1}PbI_3$ films prepared at various reaction temperatures. The XRD peaks assigned to α-phase, δ-phase, PbI_2 and FTO substrates are marked with solid circles, δ, open circles and asterisks, respectively.

Five reaction temperatures (120 °C, 140 °C, 160 °C, 180 °C and 200 °C, respectively) are applied to study the effect of temperature in the formation of $FAPbI_3$ and $FA_{0.9}Cs_{0.1}PbI_3$. The XRD patterns of $FAPbI_3$ and $FA_{0.9}Cs_{0.1}PbI_3$ films prepared at various reaction temperatures are shown in Fig. S1**.** As shown in Fig. S1(a), a set of strong diffraction peaks, which belong to α-phase $FAPbI_3$ are marked with solid circles. Besides, an extra strong peak at 12.65° exists in the XRD patterns of the $FAPbI_3$ film prepared at 120 °C, which belongs to the unreacted PbI_2. Furthermore, a set of diffraction peaks, which are marked with δ, indicate the existence of δ-phase $FAPbI_3$. The diffraction peaks of PbI_2 and δ-phase $FAPbI_3$ still exist at the reaction temperature of 140 °C, and finally disappear at 160 °C. Moreover, at reaction temperatures of 180 °C and 200 °C, PbI_2 characteristic peak reappears, which comes from the thermal

decomposition of $FAPbI_3$ at the high temperatures. As shown in Fig. S1(b), the diffraction peaks of PbI_2 and δ-phase $FA_{0.9}Cs_{0.1}PbI_3$ also exist at 120 °C, but the intensity is low. After increasing the reaction temperature to 140 °C, no δ-phase $FA_{0.9}Cs_{0.1}PbI_3$ diffraction peak can be found. Furthermore, pure α-phase $FA_{0.9}Cs_{0.1}PbI_3$ is obtained at both 160 °C and 180 °C. After increasing the reaction temperature to 200 °C, weak diffraction peak of PbI_2 appears, which indicates a slight decomposition of $FA_{0.9}Cs_{0.1}PbI_3$. The XRD analysis indicates that $FA_{0.9}Cs_{0.1}PbI_3$ has lower phase translation temperature and higher thermal decomposition temperature than $FAPbI_3$. Therefore, Cs^+ incorporation enhances the stability of α-phase and broadens the range of reaction temperature for preparing $FA_{1-x}Cs_xPbI_3$ materials.

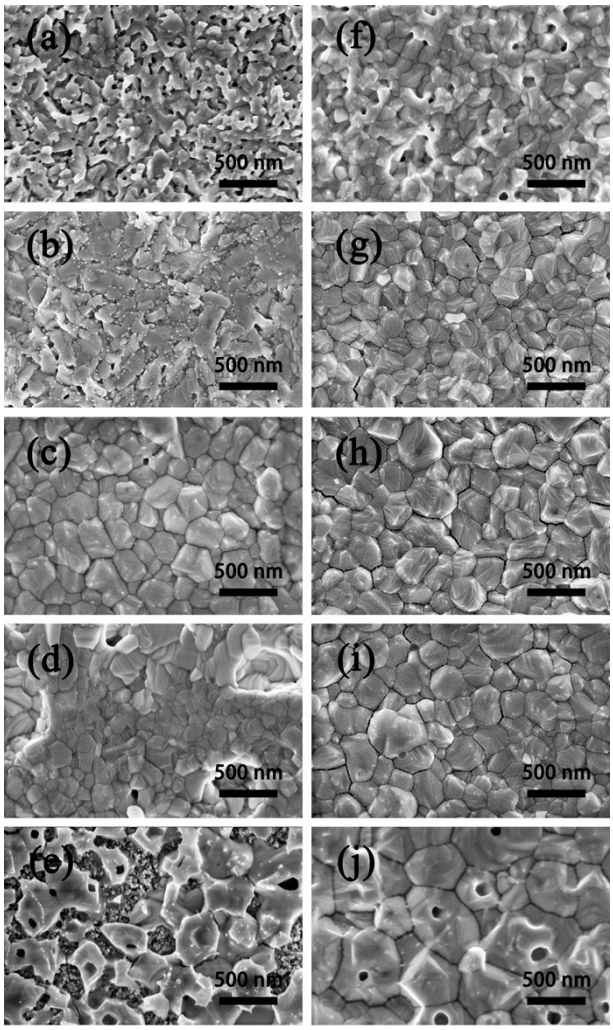

Fig. S2 SEM images of the $FAPbI_3$ and $FA_{0.9}Cs_{0.1}PbI_3$ films prepared at various reaction temperatures. For $FAPbI_3$, (a) 120 °C, (b) 140 °C, (c) 160 °C, (d) 180 °C and (e) 200 °C, respectively. For $FA_{0.9}Cs_{0.1}PbI_3$, (f) 120 °C, (g) 140 °C, (h) 160 °C, (i) 180 °C and (j) 200 °C, respectively.

SEM images of the $FAPbI_3$ and $FA_{0.9}Cs_{0.1}PbI_3$ films prepared at different reaction temperatures are shown in Fig. S2. Fig. S2(a) shows the $FAPbI_3$ film prepared at 120 ^oC, which exhibits poor crystallinity with pin-hole defects. With the increasing of reaction temperature, the $FAPbI_3$ grains grow up. At the reaction temperature of 160 ^oC, the $FAPbI_3$ film exhibits improved crystallinity with compact structure (Fig. S2(c)). By further increasing the reaction temperature, some hole defects emerged in the film at 180 ^oC and the film shows poor coverage at 200 ^oC (Fig. S2(d) and S2(e)). Fig. S2(f) shows the morphology of $FA_{0.9}Cs_{0.1}PbI_3$ film prepared at 120 ^oC, which has poor crystallinity with pin-hole defects. Comparing with the $FAPbI_3$ films prepared at the same temperature, the crystallinity of $FA_{0.9}Cs_{0.1}PbI_3$ films has been improved. After increasing the reaction temperature to 140 ^oC, the prepared $FA_{0.9}Cs_{0.1}PbI_3$ film has a compact structure with well crystallization (Fig. S2(g)). Further increasing the reaction temperature to 160 ^oC and 180 ^oC, the grain size slightly increases and the compact structure preserves in Fig. S2(h) and S2(i). In Fig. S2(j), hole defects appear on the $FA_{0.9}Cs_{0.1}PbI_3$ grains at the reaction temperature of 200 ^oC, which is likely due to the decomposition of $FA_{0.9}Cs_{0.1}PbI_3$. Therefore, well crystallized light harvester films without hole defects can be prepared in the reaction temperature range of 140 ^oC to 180 ^oC for $FA_{0.9}Cs_{0.1}PbI_3$, which is broader than the reaction temperature range of $FAPbI_3$ (around 160 ^oC).

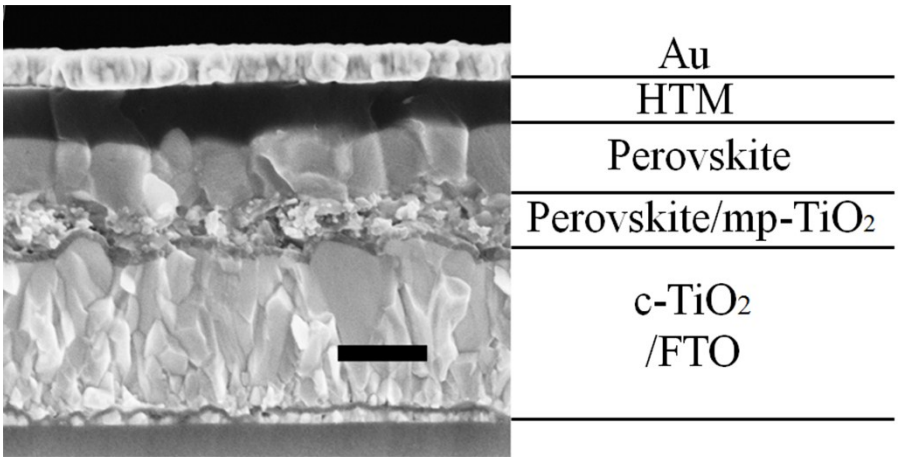

Fig. S3 Cross-sectional SEM image of the device with $FA_{0.9}Cs_{0.1}PbI_3$ light harvester, mp-TiO_2 represents the mesoporous TiO_2 layer penetrated with $FA_{0.9}Cs_{0.1}PbI_3$, c-TiO_2 represents the compact TiO_2 layer, the scale bar is 300 nm.

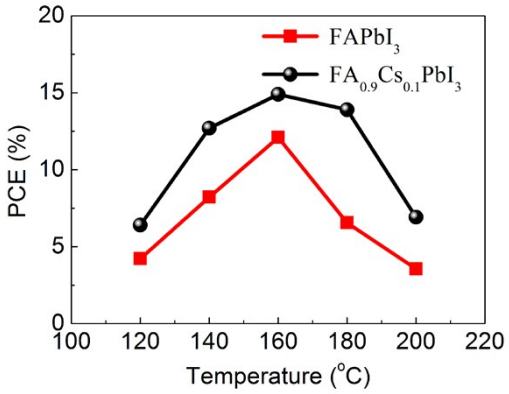

Fig. S4 The PCEs of the devices based on the $FAPbI_3$ and $FA_{0.9}Cs_{0.1}PbI_3$ films prepared at various reaction temperatures.

Table S1 EDS measurements of $FA_{1-x}Cs_xPbI_3$ (x=0, 0.1, 0.2 and 0.3) solid solution films.

Element	x=0		x=0.1		x=0.2		x=0.3	
	wt%[a]	atom%[b]	wt%	atom%	wt%	atom%	wt%	atom%
Cs	0.00	0.000	5.75	0.095	11.76	0.207	15.29	0.281
Pb	100.00	1	94.25	1	88.24	1	84.71	1

[a]The weight ratio of elements. [b]The normalized mole ratio of Cs to Pb.

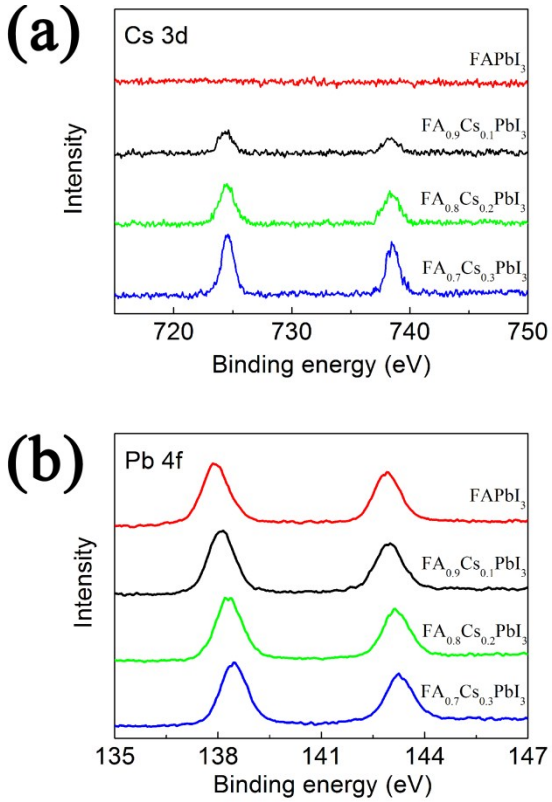

Fig. S5 (a) Cs 3d and (b) Pb 4f XPS spectra of $FA_{1-x}Cs_xPbI_3$ films.

Table S2 The ratio of Cs to Pb deduced from XPS measurements of $FA_{1-x}Cs_xPbI_3$ films.

Perovskite	$FAPbI_3$	$FA_{0.9}Cs_{0.1}PbI_3$	$FA_{0.8}Cs_{0.2}PbI_3$	$FA_{0.7}Cs_{0.3}PbI_3$
Cs/Pb[a]	0:1	0.09:1	0.18:1	0.29:1

[a]The normalized mole ratio of Cs to Pb.

The XPS spectra were performed by VG scientat XPS system. XPS spectra of $FA_{1-x}Cs_xPbI_3$ films are shown in Fig. S5. In Fig. S5(a), the peak intensity of Cs element increases with the increase of Cs^+ ion incorporation in the $FA_{1-x}Cs_xPbI_3$ films. We estimate the mole ratio of Cs element to Pb element by the peak intensity in the XPS spectra, the result is summarized in Table S2. It illustrates that our preparation method can effectively control the concentration of Cs^+ ions in the $FA_{1-x}Cs_xPbI_3$ films. Fig. S5(b) also indicates that binding energy of Pb element increases with the increase of Cs ion concentration. We think it may relate with the decrease of lattice parameters by Cs ion incorporation.

Table S3 Lattice parameters of $FA_{1-x}Cs_xPbI_3$ with trigonal structure summarized from XRD patterns.

Perovskite	a (nm)	b (nm)	c (nm)
$FAPbI_3$	0.895	0.895	1.099
$FA_{0.9}Cs_{0.1}PbI_3$	0.892	0.892	1.096
$FA_{0.8}Cs_{0.2}PbI_3$	0.890	0.890	1.093
$FA_{0.7}Cs_{0.3}PbI_3$	0.888	0.888	1.091

The lattice parameters of $FA_{1-x}Cs_xPbI_3$ with trigonal structure obtained from the corresponding XRD patterns are summarized in Table S3. It can be seen that the lattice parameters decrease with the increase of Cs^+ ion concentration.

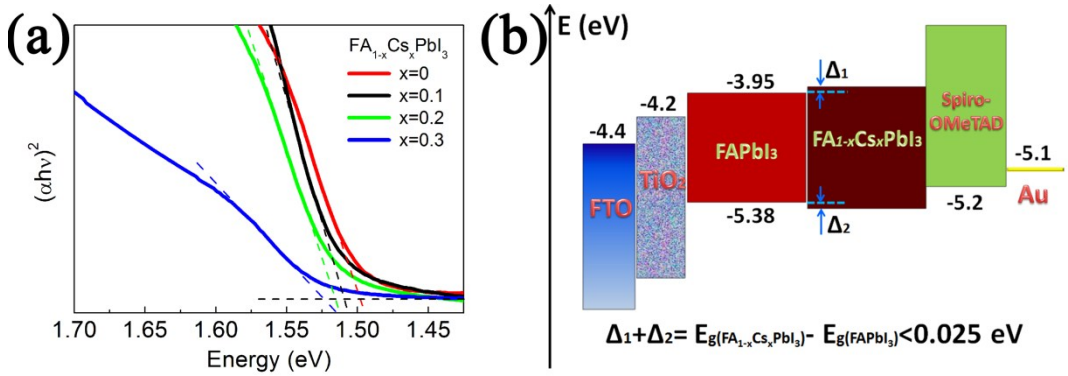

Fig. S6 (a) The absorption band edge position of the $FA_{1-x}Cs_xPbI_3$ (x=0, 0.1, 0.2, 0.3) films. (b) Schematic energy level diagram of each layer in the perovskite solar cells.

Table S4 The energy band gap of the $FA_{1-x}Cs_xPbI_3$ (x=0, 0.1, 0.2, 0.3) films.

Perovskite	$FAPbI_3$	$FA_{0.9}Cs_{0.1}PbI_3$	$FA_{0.8}Cs_{0.2}PbI_3$	$FA_{0.7}Cs_{0.3}PbI_3$
Energy gap (eV)	1.498	1.509	1.515	1.523

Cui et al measured the energy band edge positions of $FAPbI_3$ material by the optical absorbance spectra and the photo electron spectroscopy[1]. In their report, the conduction band edge position of $FAPbI_3$ is -3.95 eV and the valence band edge position of $FAPbI_3$ is -5.38 eV. The conduction band edge position of TiO_2 is -4.2 eV, which is 0.25 eV lower than that of $FAPbI_3$[2]. The valence band edge position of OMeTAD is -5.2 eV, which is 0.18 eV higher than that of $FAPbI_3$[2]. We estimate the energy band gaps of $FA_{1-x}Cs_xPbI_3$ films by the

absorption band edge position according to Kubellka−Munk equation. The difference of band gap is less than 0.025 eV in the $FA_{1-x}Cs_xPbI_3$ films with these four Cs^+ ion concentrations. And the band gap of $FA_{0.9}Cs_{0.1}PbI_3$ is only 0.011 eV larger than that of $FAPbI_3$. The increase of band gap usually comes from the increase of conduction band edge position and the decrease of valence band edge position. The above analysis shows that the increase of band gap for $FA_{1-x}Cs_xPbI_3$ films is much lower than the band edge position difference at TiO_2/$FAPbI_3$ and $FAPbI_3$/OMeTAD interfaces. Therefore, we think the movement of band edge position does not remarkably change the energy level alignment at interfaces in the devices based on these $FA_{1-x}Cs_xPbI_3$ with different Cs^+ ion concentration.

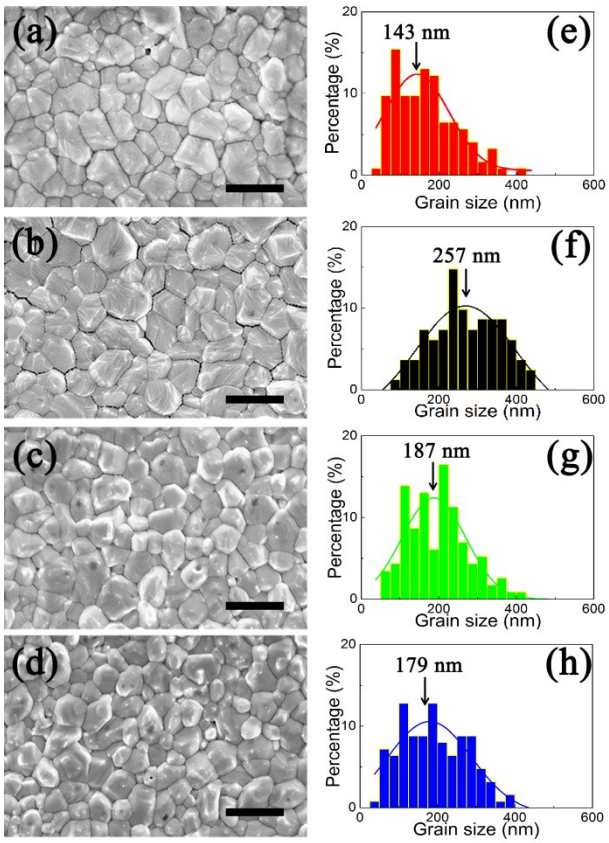

Fig. S7 SEM images and grain size distributions of $FAPbI_3$ (a, e), $FA_{0.9}Cs_{0.1}PbI_3$ (b, f), $FA_{0.8}Cs_{0.2}PbI_3$ (c, g) and $FA_{0.7}Cs_{0.3}PbI_3$ (d, h) films on FTO substrates with TiO_2 porous layers, respectively.

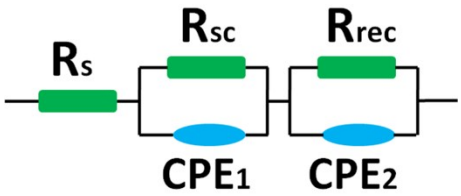

Fig. S8 Equivalent circuit for fitting the impedance spectra.

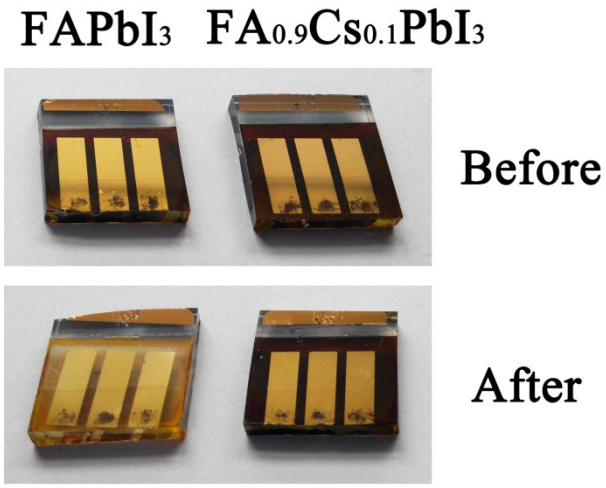

Fig. S9 Photographs of the $FAPbI_3$-based and $FA_{0.9}Cs_{0.1}PbI_3$-based devices before and after 100 hours aging in 50% humidity and 20 °C environment.

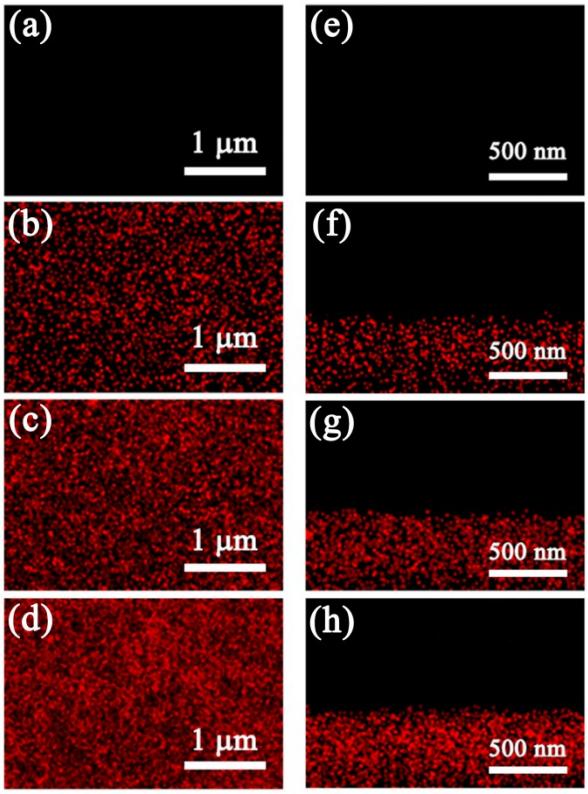

Fig. S10 EDS mapping of Cs element in the $FA_{1-x}Cs_xPbI_3$ films with different Cs ion concentrations by plane scan (a~d) and cross-sectional scan (e~h). (a, e) $FAPbI_3$, (b, f) $FA_{0.9}Cs_{0.1}PbI_3$, (c, g) $FA_{0.8}Cs_{0.2}PbI_3$ and (d, h) $FA_{0.7}Cs_{0.3}PbI_3$, respectively.

The EDS mapping of Cs element is shown in Fig. S10, which obtained with the same measurement condition for the $FA_{1-x}Cs_xPbI_3$ films with four different Cs ion concentrations. Fig. S10(a~d) shows the plane distribution of Cs element in $FA_{1-x}Cs_xPbI_3$ films. It can be seen that Cs element is homogeneously distributed in the $FA_{1-x}Cs_xPbI_3$ film. Moreover, the signal intensity of Cs element increases with the increase of Cs incorporation. Fig. S10(e~h) shows the cross-sectional distribution of Cs element in the $FA_{1-x}Cs_xPbI_3$ film. The bottom parts (about 200 nm thickness) show a relatively low signal intensity of Cs element, which is due to the existence of TiO_2 porous layer. Moreover, Cs element is also homogeneously distributed in the depth direction of the capping layer of $FA_{1-x}Cs_xPbI_3$.

Table S5 The statistics of the photovoltaic parameters of $FAPbI_3$-based and $FA_{0.9}Cs_{0.1}PbI_3$-based solar cells before and after 100 h aging.

Perovskite	Aging time (h)	J_{sc} (mA/cm^2)	V_{oc} (V)	Fill factor	PCE (%)
$FAPbI_3$	0	17.1±0.8	0.96±0.02	0.63±0.02	10.4±0.8
	100	0.78±0.30	0.94±0.02	0.57±0.06	0.42±0.17
$FA_{0.9}Cs_{0.1}PbI_3$	0	20.6±0.5	1.05±0.01	0.68±0.02	14.7±0.3
	100	17.7±0.6	1.01±0.01	0.65±0.02	11.7±0.7

In the humidity stability test, the perovskite solar cells are not encapsulated and kept in dark condition. The devices are aged in the environment of 50% humidity at 20 °C for 100 h.

The statistics of the photovoltaic parameters are summarized in Table S5. For both $FAPbI_3$-based and $FA_{0.9}Cs_{0.1}PbI_3$-based solar cells, the parameters are obtained from five devices before and after 100 h aging in the environment of 50% humidity at 20 °C. The average efficiency of $FAPbI_3$-based devices decreases from 10.4% to 0.42% after the 100 h aging. However, $FA_{0.9}Cs_{0.1}PbI_3$-based devices still obtain an average efficiency of 11.7% after the aging test. It indicates that Cs^+ ions incorporation can enhance the stability of the devices.

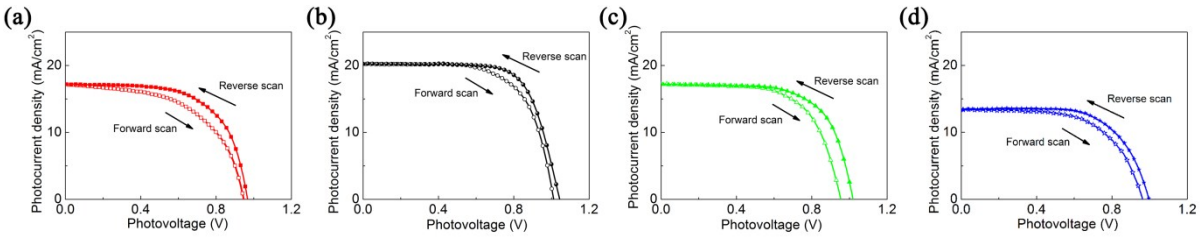

Fig. S11 The photocurrent density-photovoltage characteristic of the devices via different scanning directions. Reverse scan is the first scan direction (from 1.1 V to 0 V). (a) $FAPbI_3$, (b) $FA_{0.9}Cs_{0.1}PbI_3$, (c) $FA_{0.8}Cs_{0.2}PbI_3$ and (d) $FA_{0.7}Cs_{0.3}PbI_3$, respectively.

Table S6 The photovoltaic parameters of the devices based on $FA_{1-x}Cs_xPbI_3$ (x=0, 0.1, 0.2 and 0.3).

Perovskite	Scan	Jsc (mA/cm^2)	Voc (V)	Fill factor	PCE (%)
$FAPbI_3$	Reverse	17.2	0.97	0.62	10.4
	Forward	17.2	0.95	0.54	8.9
$FA_{0.9}Cs_{0.1}PbI_3$	Reverse	20.3	1.05	0.70	14.9
	Forward	20.3	1.02	0.65	13.5
$FA_{0.8}Cs_{0.2}PbI_3$	Reverse	17.1	1.02	0.66	11.5
	Forward	17.1	0.96	0.63	10.4
$FA_{0.7}Cs_{0.3}PbI_3$	Reverse	13.4	0.99	0.66	8.7
	Forward	13.4	0.96	0.61	7.8

The PCE via forward scan of the devices based on $FA_{1-x}Cs_xPbI_3$ (x=0, 0.1, 0.2 and 0.3) is 14.4%, 9.4%, 9.6% and 10.3% lower than the PCE via reverse scan, respectively. It indicates that Cs-doping can slightly mitigate hysteresis.

Refecence

S1 S. Pang, H. Hu, J. Zhang, S. Lv, Y. Yu, F. Wei, T. Qin, H. Xu, Z. Liu and G. Cui, *Chem. Mater.,* 2014, **26**, 1485.

S2 J. Rhee, C. Chung and E. Diau, *NPG Asia Mater.*, 2013, **5**, e68.